Structural Engineering and Mechanics, *Vol. 72, No. 2 (2019) 141-153*
DOI: https://doi.org/10.12989/sem.2019.72.2.141

Earthquake response of roller compacted concrete dams including galleries

Muhammet Karabulut[1a] and Murat Emre Kartal*[2]

[1]*Department of Civil Engineering, Zonguldak Bulent Ecevit University, Zonguldak, Turkey*
[2]*Department of Civil Engineering, Engineering Faculty, Izmir Democracy University, Izmir, Turkey*

(Received February 26, 2019, Revised May 2, 2019, Accepted May 22, 2019)

Abstract. The effect of galleries on the earthquake behavior of dams should be investigated to obtain more realistic results. Therefore, a roller compacted concrete (RCC) dam with and without galleries are examined under ground motion effects. For this purpose, Cine RCC dam constructed in Aydın, Turkey, is selected in applications. The optimal mesh around galleries is investigated to obtain the most realistic results. Two-dimensional finite element models of Cine RCC dam with and without galleries are prepared by using ANSYS software. Empty and full reservoir conditions were taken into account in the time-history analyses. Hydrodynamic effect of the reservoir water was taken into account considering two-dimensional fluid finite elements based on the Lagrangian approach. It is examined that how principle stresses and displacements change by height and during earthquake. The dam-foundation-reservoir interaction was taken into consideration with contact-target element pairs. The displacements and principle stress components obtained from the linear analyses are compared each other for various cases of reservoir water and galleries. According to numerical analyses, the effect of galleries is clear on the response of RCC dam. Besides, hydrodynamic water effect obviously increases the principle stress components and horizontal displacements of the dam.

Keywords: Dynamic analysis of dams; gallery; Lagrangian approach; mesh optimization; roller compacted concrete dam

1. Introduction

Dams are one of the largest structural types. These huge structures can even lead to some disasters even in a stable condition. For example, water accumulating in the reservoir can cause seismic movements. For this reason, dams should be thoroughly analyzed from all aspects. Roller compacted concrete (RCC) dams are designed as conventional concrete structures. But the construction methods, concrete mix design, and details of the appurtenant structures are different in these structures. The construction techniques utilized in RCC dams are analogous to those used for embankment dams. These techniques provide rapid placement and economically advantages for construction. RCC dams are relatively dry, lean, zero slump concrete material containing coarse and fine aggregate that is consolidated by external vibration using vibratory rollers, dozer, and other heavy equipment. Construction procedures associated with RCC require particular attention to be given in the layout and design to water tightness and seepage control, horizontal and transverse joints, facing elements, and appurtenant structures. In the hardened condition, mechanical properties of RCC dams take after those of conventional concrete dams (USACE, 1995).

Researchers usually focused on the thermal analysis of RCC dams because thermal cracking may create a leakage path from upstream face to downstream side that is aesthetically undesirable. Noorzaei *et al.* (2006) performed thermal and structural analysis of Kinta RCC gravity dam, which is the first RCC dam in Malaysia, using the developed two-dimensional finite element code. Then the authors compared predicted temperatures obtained from the finite element code with actual temperatures measured in the field using thermocouples installed within the dam body. They found some results in good agreement with them. Jaafar *et al.* (2007) developed a finite element based computer code to determine the temperatures within the dam body. According to performed thermal analysis of a RCC dam changing the placing schedule can optimize the locations of maximum temperature zones. Abdulrazeg *et al.* (2010) performed three dimensional coupled thermal and structural analysis of roller compacted concrete dams. Abdulrazeg *et al.* assessed crack development within the dam body using the proposed crack index. This method remarkably reduces the total number of elements and nodes when the dam height was increased. Zhang *et al.* (2011) simulated and analyzed the temperature field and thermal stress of certain RCC gravity dams in cold regions using the material properties of roller-compacted concrete by three-dimensional finite element relocating mesh method. As a result, the authors indicated that superficial insulation prevented surface cracks from forming.

Zhuang *et al.* (2018) study on crack formation and propagation in the galleries of the Dagangshan high arch dam in Southwest China. To investigate crack formation and propagation in the galleries of the high arch dam, micro seismic monitoring and 3D finite element analysis of the galleries were performed during the filling process. Cracking may occur in the gallery close to the dam toe if its

*Corresponding author, Professor
E-mail: murat.kartal@idu.edu.tr
[a] Ph.D. Student

ISSN: 1225-4568 (Print), 1598-6217 (Online)

microseismicity continues increasing. Kianoush *et al.* (2009) investigated damage mechanics approach and modeling nonuniform cracking for safety evaluation of concrete dams. Morrow Point dam is analyzed including dam-reservoir interaction effects to consider the nonlinear seismic behavior of the dam. It is concluded that the proposed model can be used in nonlinear static and dynamic analysis of concrete dams in 3D space and enables engineers to define the damage level of these infrastructures. Lotfi (2007) studied direct frequency domain analysis of concrete arch dams. It is show that a FE-BE procedure is presented for dynamic analysis of concrete arch dams, dam body is discretized by finite elements, while foundation rock is handled by three dimensional boundary element formulation. The partial interaction treatment (Foundation flexibility only) can model the shift in the natural frequencies correctly. However, the amplitude of the response is not estimated correctly, and the trend in change of response is actually opposite to the true behavior.

Moradloo *et al.* (2018) focused on seismic fragility evaluation of arch concrete dams. Amirkabir arch concrete dam was subjected to non-linear dynamic analyses. The results indicate that displacement damages index is more conservative and impractical in the fragility analysis than tensional damage index. Bayagoob *et al.* (2010) studied coupled thermal and structural analysis of roller compacted concrete arch dam. The Ostour Arch dam located on Ghezel-Ozan River, Iran, which was originally designed as conventional concrete arch dam, has been taken for the purpose of verication of the finite element code. It was seen that there is an increase in the tensile stresses after five years over stresses obtained immediately at the end of construction by 61.3%. Sevim (2018) investigated geometrical dimension effects on the seismic response of concrete gravity dams. In the study, a concrete gravity dam with the height of 200 m is selected and finite element models of the dam are constituted including five different L/H ratios such as 0.25, 0.5, 0.75, 1.00, 1.25. The results show that the L/H ratios considerably affect the seismic response of gravity dams.

Akpınar *et al.* (2014) studied earthquake stresses and effective damping in concrete gravity dams. The maximum principal tensile stresses and their distribution at the dam base, which are important parameters for concrete dam design, were obtained using the frequency domain approach. A new effective damping prediction equation was proposed in order to estimate earthquake stresses accurately with the approximate time domain approach. Yang *et al.* (2017) investigated a comprehensive evaluation method study for dam safety. According to the multi-index system of dam safety assessment and the standard of safety, a comprehensive evaluation model for dam safety based on a cloud model is established to determine the basic probability assignment of the Dempster-Shafer theory. The rationality and feasibility of the model are verified through application to the safety evaluation of a practical arch dam. Su *et al.* (2016) studied fractal behavior identification for monitoring data of dam safety. According to the prototypical observations, the correct identification on above nonlinear characteristics is very important for dam safety control. It is indicated that the mechanism evidence can be provided for the prediction and diagnosis of dam structural behavior by using the fractal identification method. Akköse (2016) focused on arrival direction effects of travelling waves on nonlinear seismic response of arch dams. The aim of this study is to investigate arrival direction effects of travelling waves on non-linear seismic response of arch dams. Linear and non-linear dynamic response of arch dams to the earthquake ground motion is affected from several factors including interaction of the dam with the foundation rock and reservoir water, computer modelling and material properties used in the analysis. Sevim *et al.* (2013) studied structural identification of concrete arch dams by ambient vibration tests. Modal testing, widely accepted and applied method for determining the dynamic characteristics of structures for operational conditions, uses known or unknown vibrations in structures. Enhanced Frequency Domain Decomposition technique is used for the extraction of natural frequencies, mode shapes and damping ratios.

Karabulut (2016) focused on effect of galleries on two dimensional behavior of roller compacted concrete dams. As a result of the analyzes, stress increases were observed around the gallery. It has been suggested that dam modeling should be included in the galleries. Kartal and Karabulut (2018) studied earthquake performance evaluation of three-dimensional roller compacted concrete dams. A roller compacted concrete (RCC) dam should be analyzed under seismic ground motions for different conditions such as empty reservoir and full reservoir conditions. Higher tensile stresses were observed in linear analyses and then non-linear analyses were performed and compared with each other.

In the scientific studies, it is seen in the literature that the galleries are not generally included in the modeling of the dam bodies. Galleries cause a sudden loss of section and can significantly increase the stress values that may occur in the dam body. Increased stress values in case of a possible earthquake can lead to cracks in the dam body. Models with and without galleries were developed and examined for stresses and displacements. The effects of galleries on the linear earthquake response of roller compacted concrete (RCC) dams are investigated by submodelling in this paper. For this purpose, Çine RCC dam constructed in Aydın, Turkey, is selected as an application. The two dimensional finite element model of Çine RCC dam is obtained using ANSYS software. The unfavorable section of the dam is selected for two dimensional model. The material and soil mechanical properties were obtained from the experimental data of the dam. The accelerations of the Düzce 1999 earthquake were used for dynamic analysis. The aim of this study is to investigate the effect of the galleries on the dam bodies on the stresses and displacements that may occur in the dam body.

2. Formulation of Lagrangian approach for dam reservoir-foundation interaction

The formulation of the fluid system based on the Lagrangian approach is presented as following (Wilson and

Khalvati, 1983). In this approach, fluid is assumed to be linearly compressible, inviscid and irrotational. For a general two-dimensional fluid, pressure-volumetric strain relationships can be written in matrix form as follows,

$$\begin{Bmatrix} P \\ P_z \end{Bmatrix} = \begin{bmatrix} C_{11} & 0 \\ 0 & C_{22} \end{bmatrix} \begin{Bmatrix} \varepsilon_v \\ w_z \end{Bmatrix} \tag{1}$$

where P, C_{11}, and ε_v are the pressures which are equal to mean stresses, the bulk modulus and the volumetric strains of the fluid, respectively. Since irrotationality of the fluid is considered like penalty methods (Zienkiewicz and Taylor, 1989) rotations and constraint parameters are included in the pressure-volumetric strain equation (Eq. (1)) of the fluid. In this equation Pz, is the rotational stress; C_{22} is the constraint parameter and wz is the rotation about the Cartesian axis y and z.

In this study, the equations of motion of the fluid system are obtained using energy principles. Using the finite element approximation, the total strain energy of the fluid system may be written as,

$$\pi_e = \frac{1}{2} \mathbf{U}_f{}^T \mathbf{K}_f \mathbf{U}_f \tag{2}$$

where Uf and Kf are the nodal displacement vector and the stiffness matrix of the fluid system, respectively. Kf is obtained by the sum of the stiffness matrices of the fluid elements as follows,

$$\begin{aligned} \mathbf{K}_f &= \sum \mathbf{K}_f^e \\ \mathbf{K}_f^e &= \int_V \mathbf{B}_f^{e^T} \mathbf{C}_f \mathbf{B}_f^e dV^e \end{aligned} \tag{3}$$

where C_f is the elasticity matrix consisting of diagonal terms in Eq. (1) is the strain-displacement matrix of the fluid element.

An important behavior of fluid systems is the ability to displace without a change in volume. For reservoir and storage tanks, this movement is known as sloshing waves in which the displacement is in the vertical direction. The increase in the potential energy of the system because of the free surface motion can be written as,

$$\pi_s = \frac{1}{2} \mathbf{U}_{sf}^T \mathbf{S}_f \mathbf{U}_{sf} \tag{4}$$

where U_{sf} and S_f are the vertical nodal displacement vector and the stiffness matrix of the free surface of the fluid system, respectively. S_f is obtained by the sum of the stiffness matrices of the free surface fluid elements as follows,

$$\left.\begin{aligned} \mathbf{S}_f &= \sum \mathbf{S}_f^e \\ \mathbf{S}_f^e &= \rho_f g \int_A \mathbf{h}_s^T \mathbf{h}_s dA^e \end{aligned}\right\} \tag{5}$$

where h_s is the vector consisting of interpolation functions of the free surface fluid element. ρ_f and g are the mass density of the fluid and the acceleration due to gravity, respectively. Besides, kinetic energy of the system can be written as,

$$T = \frac{1}{2} \dot{\mathbf{U}}_f^T \mathbf{M}_f \dot{\mathbf{U}}_f \tag{6}$$

where $\dot{U}$ and M_f are the nodal velocity vector and the mass matrix of the fluid system, respectively. M_f is also obtained by the sum of the mass matrices of the fluid elements as follows,

$$\left.\begin{aligned} \mathbf{M}_f &= \sum \mathbf{M}_f^e \\ \mathbf{M}_f^e &= \rho_f \int_V \mathbf{H}^T \mathbf{H} dV^e \end{aligned}\right\} \tag{7}$$

where H is the matrix consisting of interpolation functions of the fluid element. If (Eq. (2), (4) and (6)) are combined using the Lagrange's equation (Clough and Penzien, 1993), the following set of equations is obtained,

$$\mathbf{M}_f \ddot{\mathbf{U}}_f + \mathbf{K}_f^* \mathbf{U}_f = \mathbf{R}_f \tag{8}$$

where $\dot{U}_f$, $\ddot{U}_f$, U_f and R_f are the system stiffness matrix including the free surface stiffness, the nodal acceleration and displacement vectors and time-varying nodal force vector for the fluid system, respectively. In the formation of the fluid element matrices, reduced integration orders are used.

The equations of motion of the fluid system, (Eq. (8)), have a similar form with those of the structure system. To obtain the coupled equations of the fluid-structure system, the determination of the interface condition is required. Since the fluid is assumed to be inviscid, only the displacement in the normal direction to the interface is continuous at the interface of the system. Assuming that the structure has the positive face and the fluid has the negative face, the boundary condition at the fluid-structure interface is,

$$U_n^- = U_n^+ \tag{9}$$

where U_c is the normal component of the interface displacement. Using the interface condition, the equation of motion of the coupled system to ground motion including damping effects are given by,

$$\mathbf{M}_c \ddot{\mathbf{U}}_c + \mathbf{C}_c \dot{\mathbf{U}}_c + \mathbf{K}_c \mathbf{U}_c = \mathbf{R}_c \tag{10}$$

in which M_c, C_c, and K_c are the mass, damping and stiffness matrices for the coupled system, respectively. $\ddot{U}_c$, $\dot{U}_c$, U_c and R_c are the vectors of the displacements, velocities, accelerations and external loads of the coupled system, respectively (Kartal 2012).

3. Mathematical model of cine RCC dam

3.1 Cine dam

Cine dam, located approximately 16km southeast of Cine, Aydın, was constructed in 2010 by General Directorate of State Hydraulic Works (Fig. 1, 2). It was

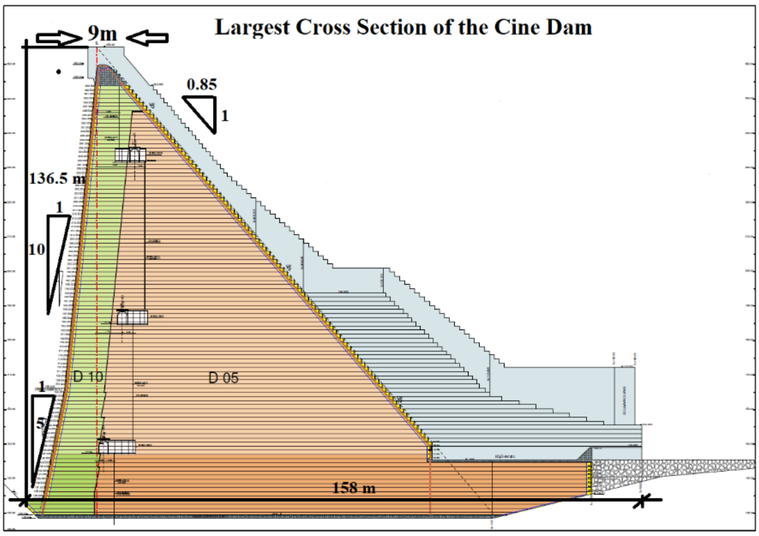

Fig. 1 The largest cross section of the Cine dam

Table 1 Material properties of Cine roller compacted concrete dam

	Material Properties					
	Modulus of elasticity (MPa)	Poisson's ratio	Mass density (kg/m^3)	Cohesion (kPa)	Angel of internal friction	Angel of dilatation
Concrete (Dam Body)	2.50E4	0.2	2500	800	41	11
Gneiss	1.75E4	0.15	2500	4000	39	9

Fig. 2 Cine Dam

established on Cine River. This dam was projected as a roller compacted concrete dam. The reservoir is used for irrigation and energy purposes. The dam crest is 372.5m in length and 9m wide. The maximum height and base width of the dam are 136.5 m and 142.5 m, respectively. The maximum height of the reservoir water is considered as 98.77 m. The annual total power generation capacity is 118 GW.

All the galleries within the dam are approximately 4 meters in height and 3 meters wide. There are three galleries in the dam body. These galleries are located at 15 meters, 52 meters and 100 meters.

3.2 Material properties of Cine RCC dam

The two-dimensional finite element model of Cine dam is modelled considering one layered foundation with gneiss rock. Material properties of Cine roller compacted concrete dam body and foundation are given in Table 1.

3.3 Finite Element Models of Cine Dam

This study considers two-dimensional finite element model (FEM) of Cine RCC dam. In this model, if the height of the dam is indicated as ‘H’, the foundation soil is extended as ‘H’ in the downstream river direction and gravity direction. Besides, foundation soil and reservoir water model is extended as “3H” in the upstream direction. Fluid and solid element matrices are computed using the Gauss numerical integration technique (Wilson and Khalvati, 1983). The solid elements have 2×2 and the fluid elements 1×1 integration points.

In this study, we modelled the RCC dam with and without galleries to observe the effect of galleries on the earthquake behaviour of the dam. The two-dimensional finite element model of Cine RCC dam is obtained using ANSYS software. The unfavourable section of the dam is selected for two dimensional model. We obtained maximum tensile and compressive stresses for the bottom point of upstream side of dam body. We investigated 4 different cases in this.

- First case excludes reservoir water and galleries. This model has 899 nodal points and 814 elements (Fig. 3).
- Second case involves full reservoir water but galleries are excluded. This model has 1130 nodal points and 1070 elements (Fig. 4).
- Third case involves galleries, empty reservoir and friction case. The friction is defined between dam and foundation. Contact elements were defined between dam and foundation. This model has 1468 elements and 1633 nodal points (Fig. 5).

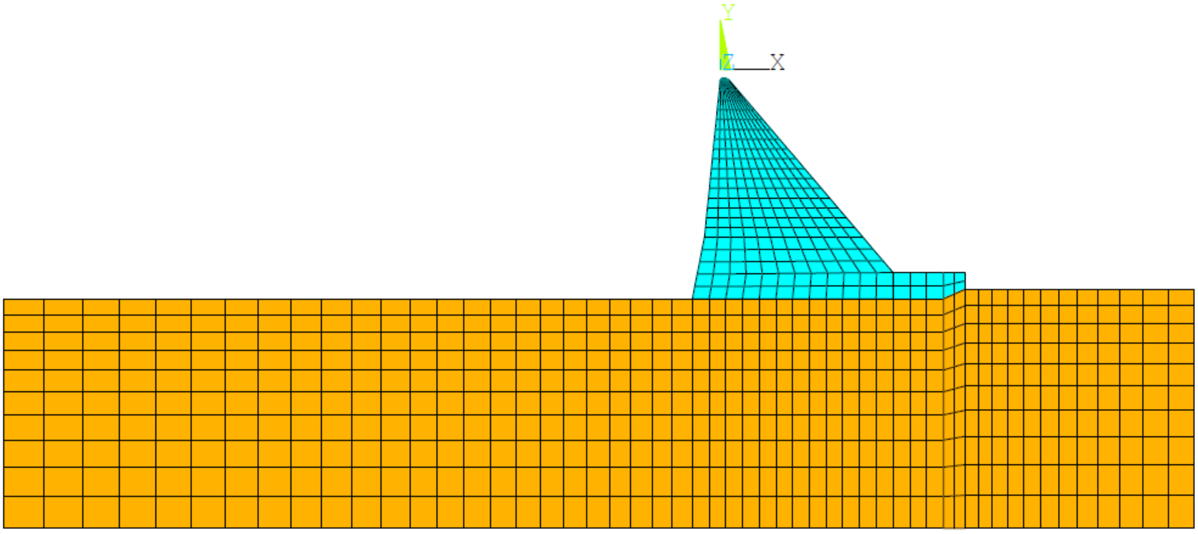

Fig. 3 FEM for empty reservoir case

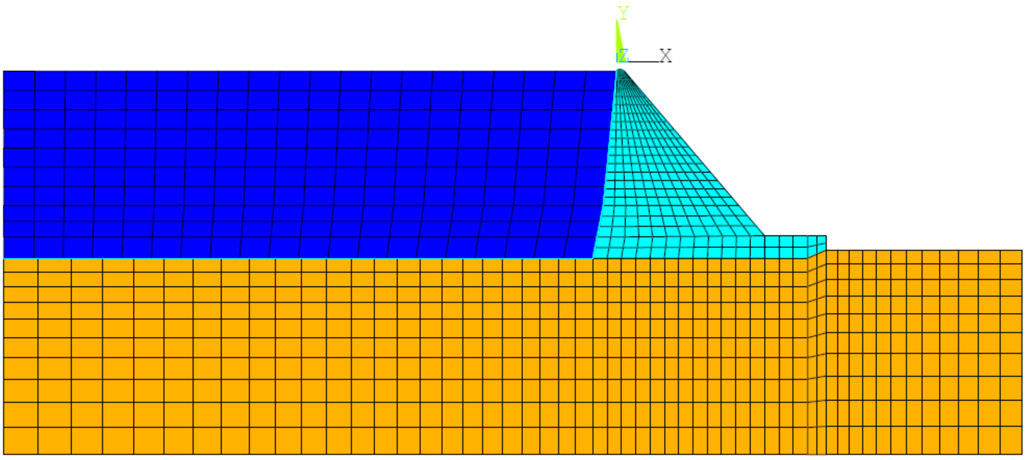

Fig. 4 FEM for full reservoir case

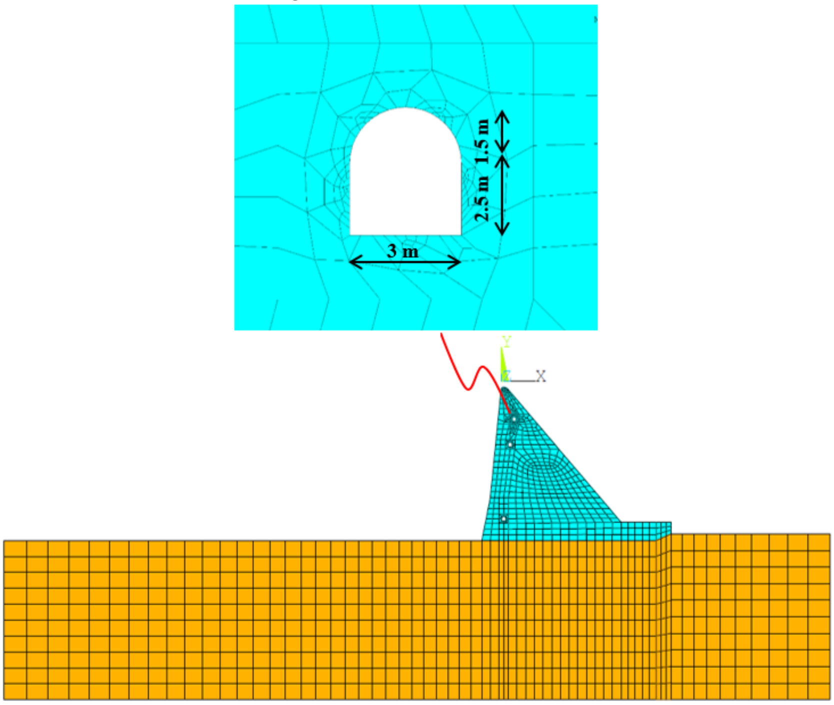

Fig. 5 FEM with galleries for empty reservoir case

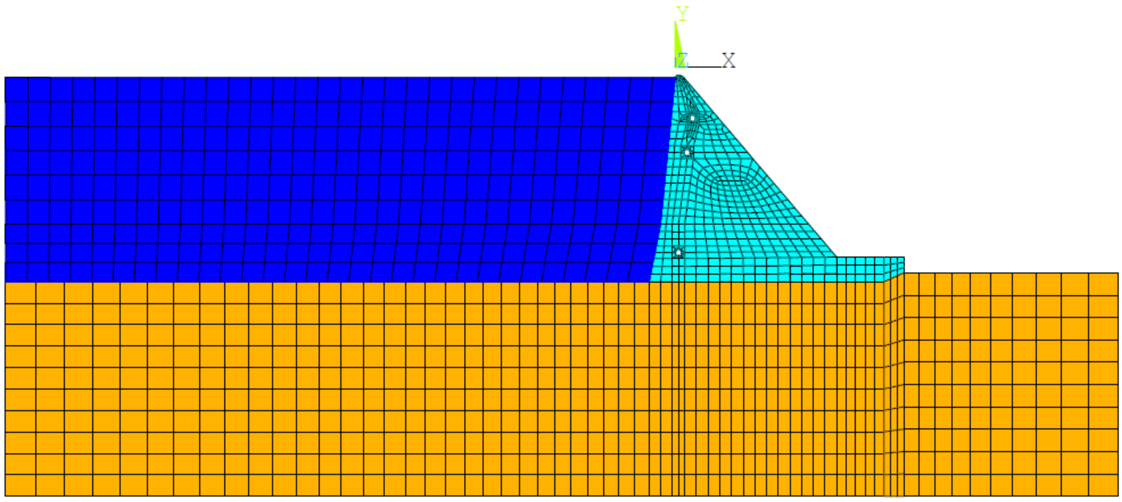

Fig. 6 FEM with galleries for full reservoir case

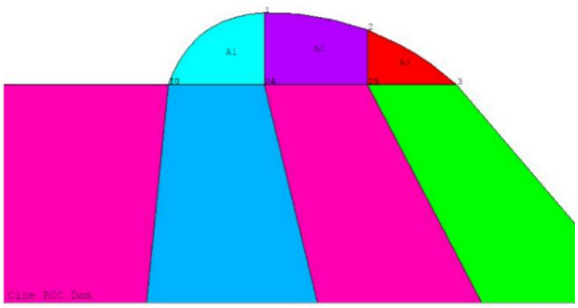

Fig. 7 FEM of the crest geometry detail

- The fourth case involves galleries, full reservoir and friction case. The friction is defined between dam and foundation. Contact elements were defined for the interaction surface. This model has 1738 elements and 1943 nodal points (Fig. 6.).

The crest of the dam body is modeled as oval in the finite element model of dam body (Fig. 7).

3.4 1999 Düzce earthquake

Almost three months after the devastating Kocaeli earthquake of August, 17, 1999, another earthquake that occurred on 12 November 1999 at 18:57 local time (16:57 UTC) with a moment magnitude of 7.2, causing damage and 1000 fatalities and 5000 injures in Düzce, Turkey. Düzce Earthquake: Epicenter: 40.768 31.148, Mb=6.5. Ms=7.3, Seismic Moment: Mo=4.5×10^{19} Nm, Mw=7.2 (Erdik, 2000). The accelerograms of the earthquake are given in Fig. 8. In this study, we used y-y direction of the Duzce accelerogram in vertical direction and z-z direction in horizontal direction.

3.5 Determination of Optimum Mesh Density

In the numerical studies, it is necessary to make the suitable finite element mesh for the realistic results. In order to determine the optimal finite element mesh, it is required to analyze the different number of finite element models

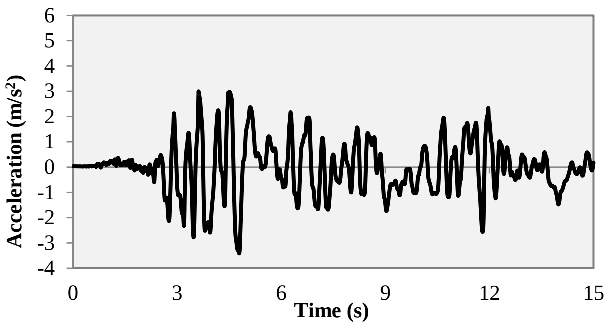

a) X-X Direction

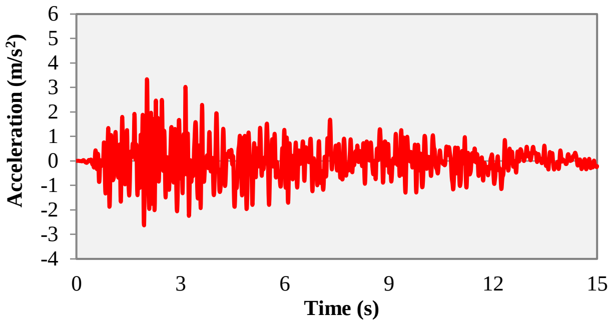

b) Y-Y Direction

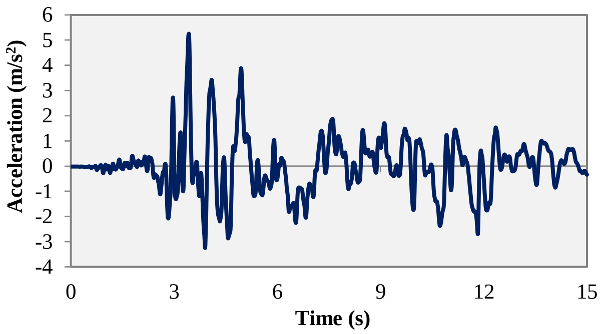

c) Z-Z Direction

Fig. 8 Duzce earthquake accelerogram

Table 2 Modal characteristics of Cine dam

Mod Number	Empty Reservoir Case		Full Reservoir Case		Empty Reservoir Case with Galleries		Full Reservoir Case with Galleries	
	Frequency (Hz)	Period (s)	Frequency(Hz)	Period (s)	Frequency(Hz)	Period (s)	Frequency(Hz)	Period (s)
1	2.3989	0.4169	2.0182	0.4955	2.4037	0.4160	2.0145	0.4964
2	4.1029	0.2437	3.7945	0.2635	4.1081	0.2434	3.8083	0.2626
3	5.4966	0.1819	5.0102	0.1996	5.4931	0.1820	5.0312	0.1988
4	9.8175	0.1019	9.2246	0.1084	9.7802	0.1022	9.2613	0.1080
5	13.1383	0.0761	11.0857	0.0902	13.1070	0.0763	11.3823	0.0879
6	14.7856	0.0676	13.0875	0.0764	14.7606	0.0677	12.6429	0.0791

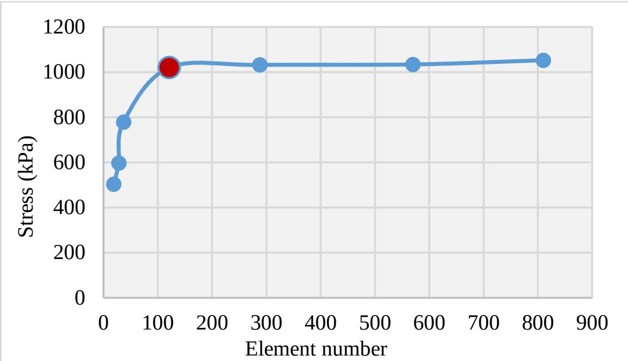

Fig. 9 Determination of optimum finite element mesh around gallery

and compare their results. The finite element mesh, which directly affects the stress values in particular, is important in places where the stresses increase suddenly. Analyzes were made with finite element meshes at different discretize to observe stress increments caused by instantaneously section loss around the gallery., the number of optimum finite elements is determined by the numerical analysis results for nearby the gallery. The numerical solutions are presented in Fig. 9.

4. Modal and dynamic analysis results

The first 6 frequencies and periods according to modal analysis for all models are given in Table 2. We investigated various evaluations for the 4 cases stated above. First one is the principle stresses changing by height of the dam (Figs. 11,12). The second one is horizontal displacements by height (Figs. 13,14). The third one is horizontal displacements during earthquake at top point of crest (Fig. 15). The fourth is maximum principle stresses around galleries are given Figs. 15-18 considering contour diagrams. And finally, the principle stresses are shown around galleries as seen Figs. 20-25.

Numerical analyses' results clearly clarify that hydrodynamic pressure of the reservoir water increases the principle stress components by dam height in upstream face. The galleries also increase these stress components by height. Furthermore, displacements undoubtedly increase by the hydrodynamic pressure effect of reservoir water by dam height. But galleries are not effective on displacements in upstream face and also in the duration of earthquake.

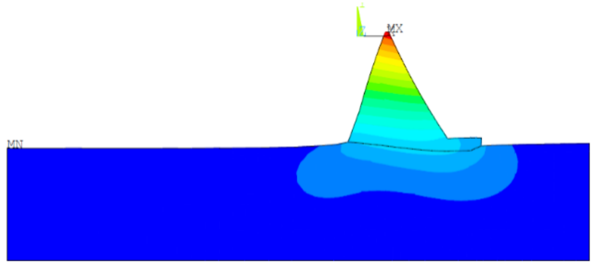

a) Empty reservoir case with no galleries (f=2.3989 Hz)

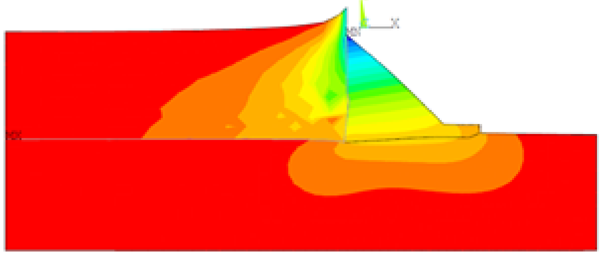

b) Full reservoir case with no galleries (f=2.0182 Hz)

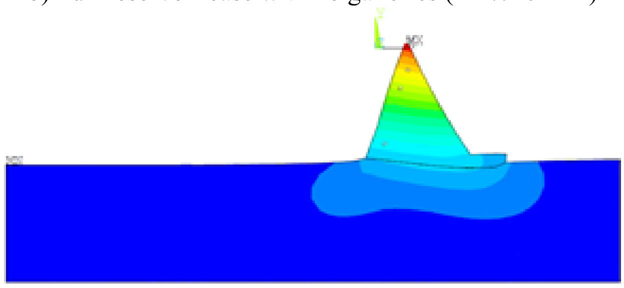

c) Empty reservoir case with galleries (f=2.4037 Hz)

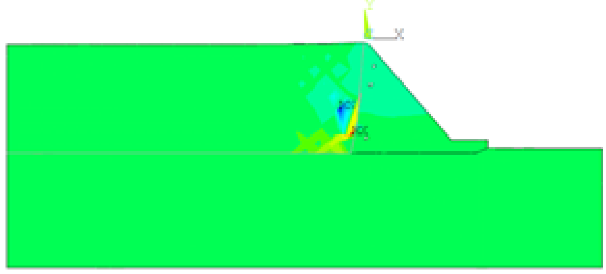

d) Full reservoir case with galleries (f=2.0145 Hz)

Fig. 10 First mod shapes of the finite element models

However, the increase of the horizontal displacements is also evident during earthquake by reservoir water effect. The contour diagrams obviously show that principle stress components have got higher values around galleries. But maximum principle stresses appear at the bottom of the dam including galleries in upstream side.

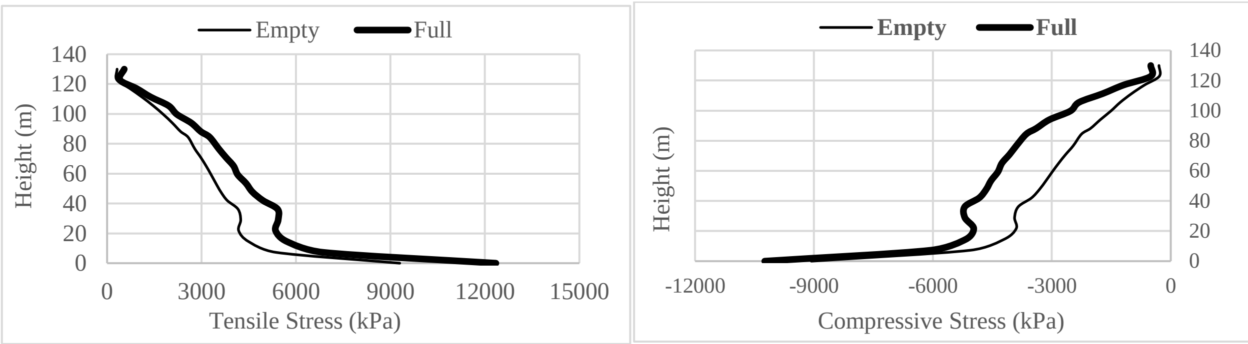

a) b)

Fig. 11 Maximum principal stresses in upstream face of the dam without galleries

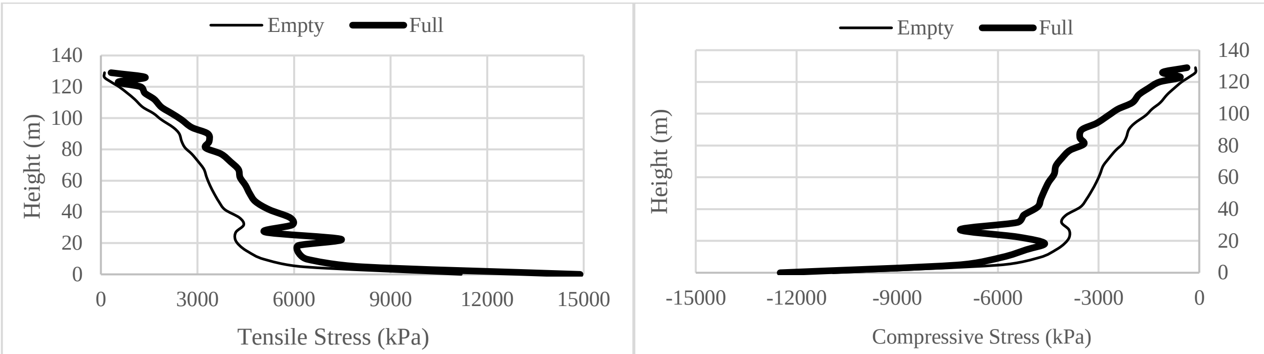

a) b)

Fig. 12 Maximum principal stresses in upstream face of the dam with galleries

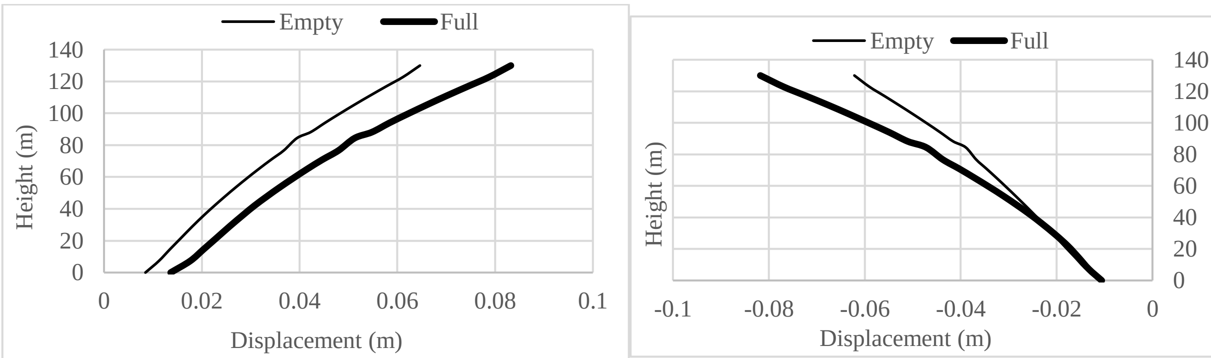

a) b)

Fig. 13 Horizontal displacements in upstream face of the dam without galleries

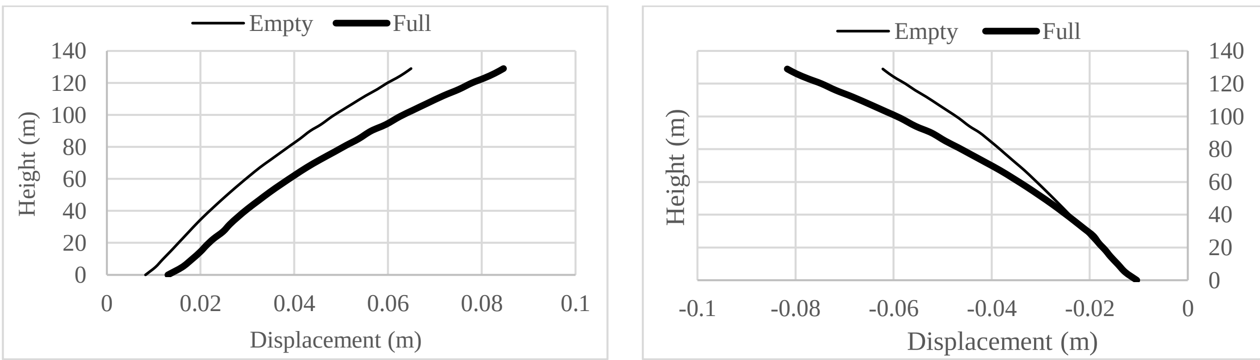

a) b)

Fig. 14 Horizontal displacements in upstream face of the dam with galleries

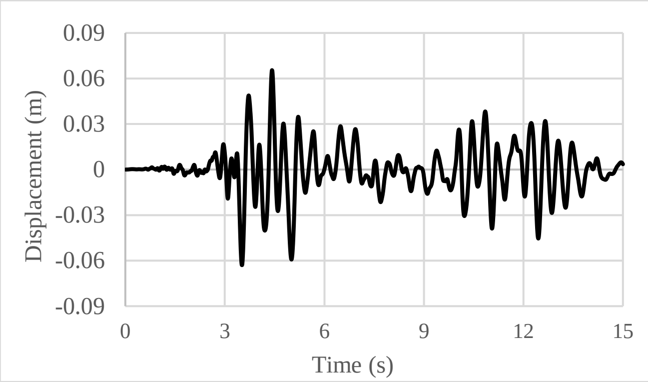

a) Empty reservoir and dam without galleries

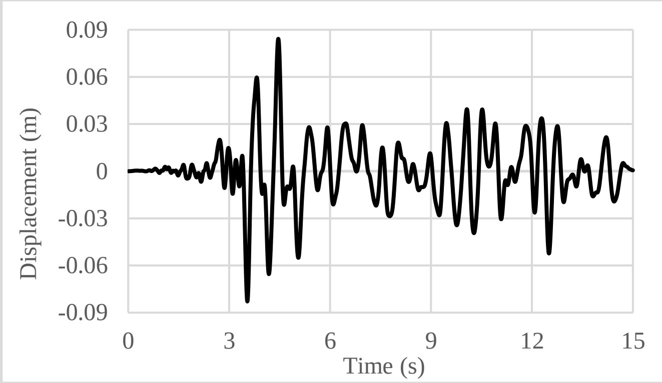

b) Full reservoir and dam without galleries

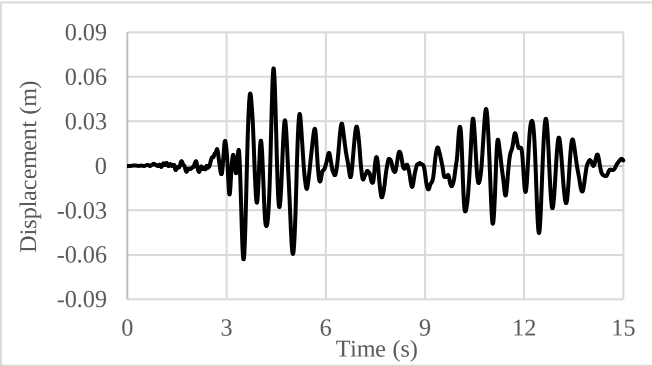

c) Empty reservoir and dam with galleries

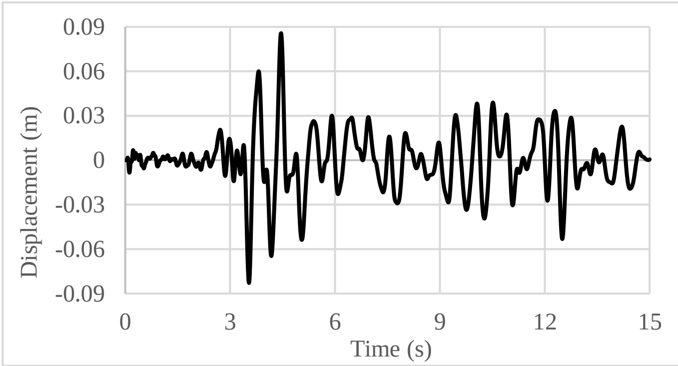

d) Full reservoir and dam with galleries

Fig. 15 Horizontal displacements during earthquake at crest

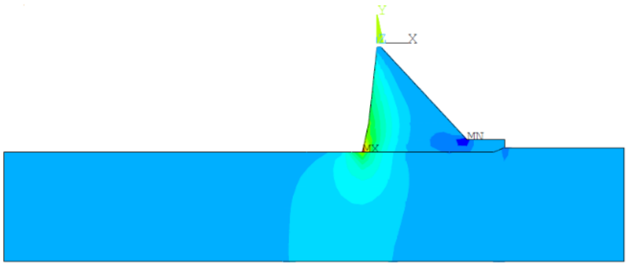

a) t=4.43 s, max. tensile stress=9294.6 kPa

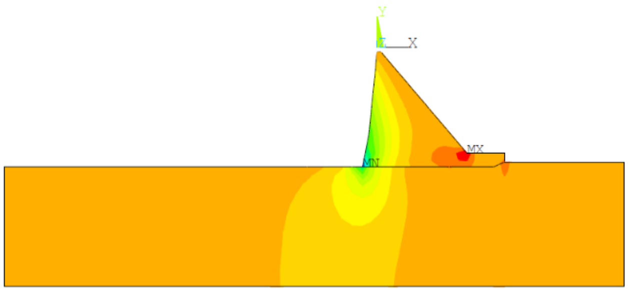

b) t= 3.51 s, max compressive stress= -9067.9 kPa

Fig. 16 Maximum principal stresses in dam without galleries and empty reservoir condition

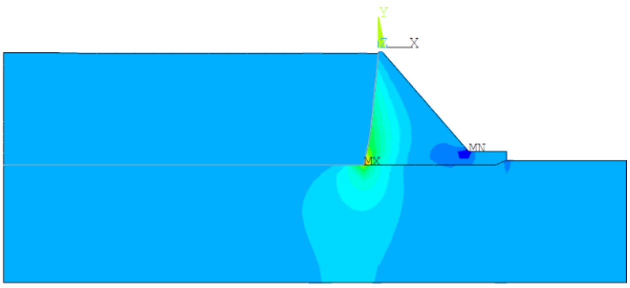

a) t= 4.45 s, max tensile stress= 12348.1 kPa

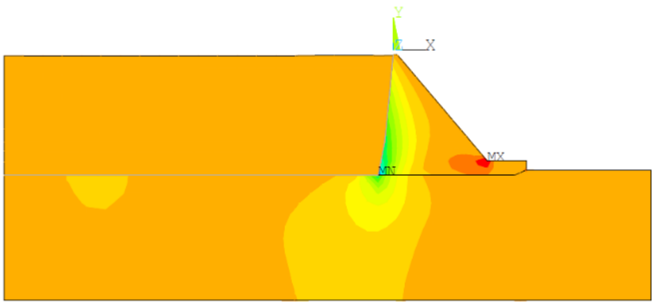

b) t= 3.52 s, max compressive stress= -10242.5 kPa

Fig. 17 Maximum principal stresses in dam without galleries and full reservoir condition

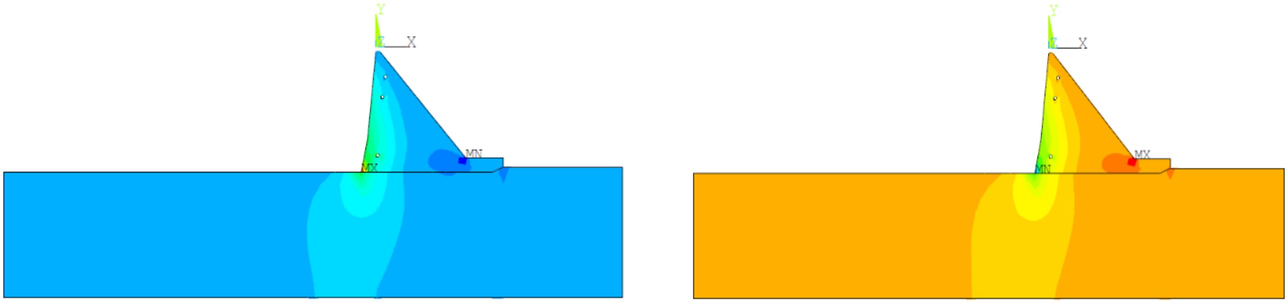

a) t= 4.44 s, max tensile stress= 11138.9 kPa   b) t= 3.51 s, max compressive stress= -10914 kPa

Fig. 18 Maximum principal stresses in dam with galleries and empty reservoir condition

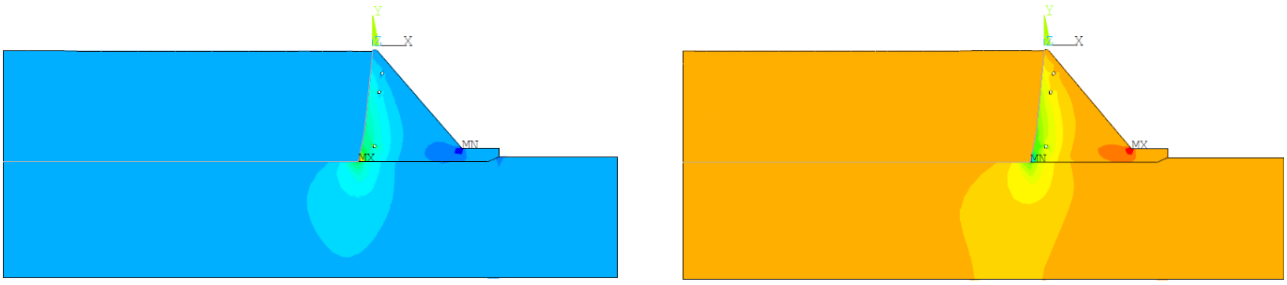

a) t= 4.44 s, max tensile stress= 14887 kPa   b) t= 3.52 s, max compressive stress= -12484.7 kPa

Fig. 19 Maximum principal stresses in dam with galleries and full reservoir condition

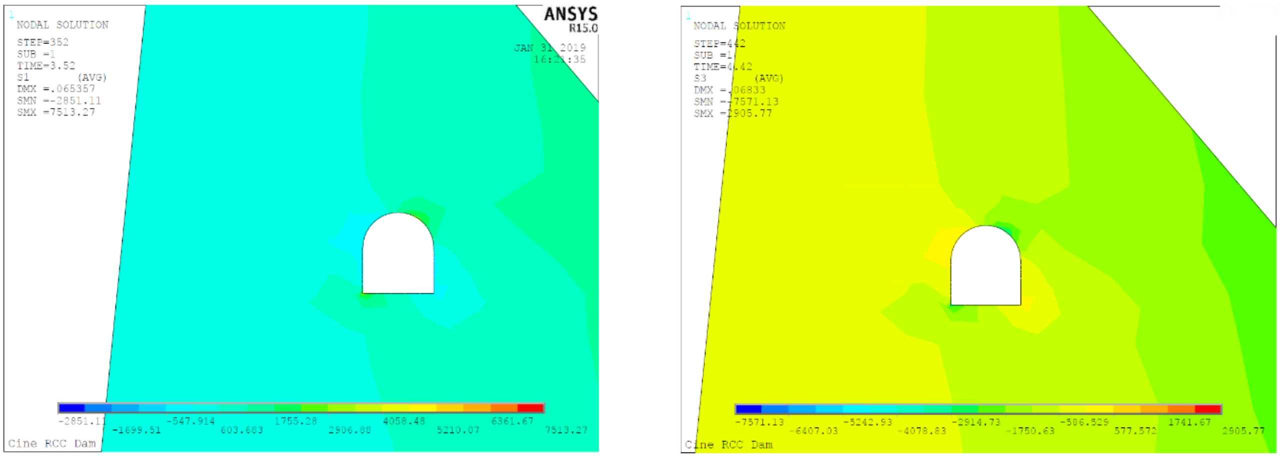

a) t= 3.52 s, max. tensile stress= 3174.6 kPa   b) t= 4.42 s, max. compressive stress= - 3552.85 kPa

Fig. 20 Maximum principal stress contour diagrams at upper gallery in empty reservoir condition.

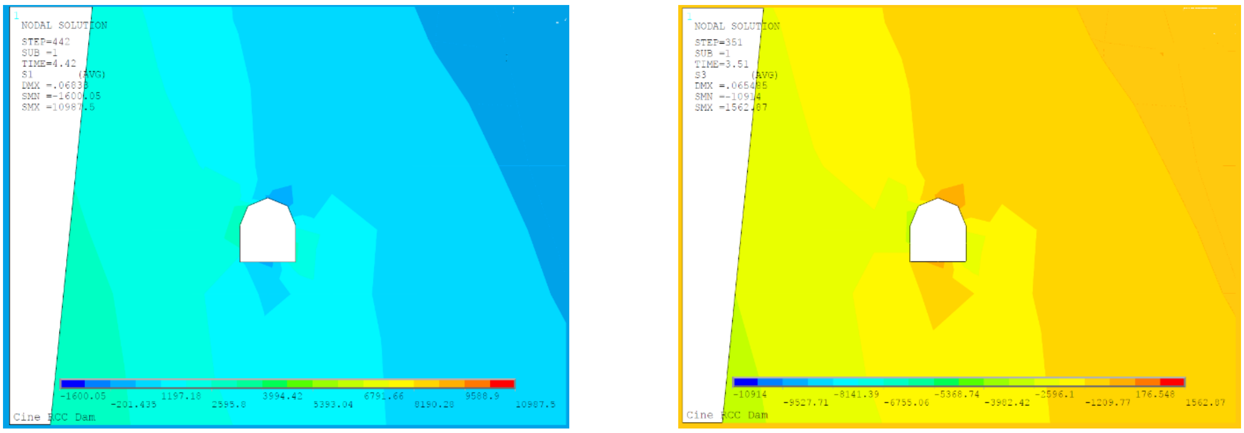

a) t= 4.43 s, max. tensile stress= 3455.1 kPa   b) t= 3.51 s, max. compressive stress= - 3142.5 kPa

Fig. 21 Maximum principal stress contour diagrams at middle gallery in empty reservoir condition

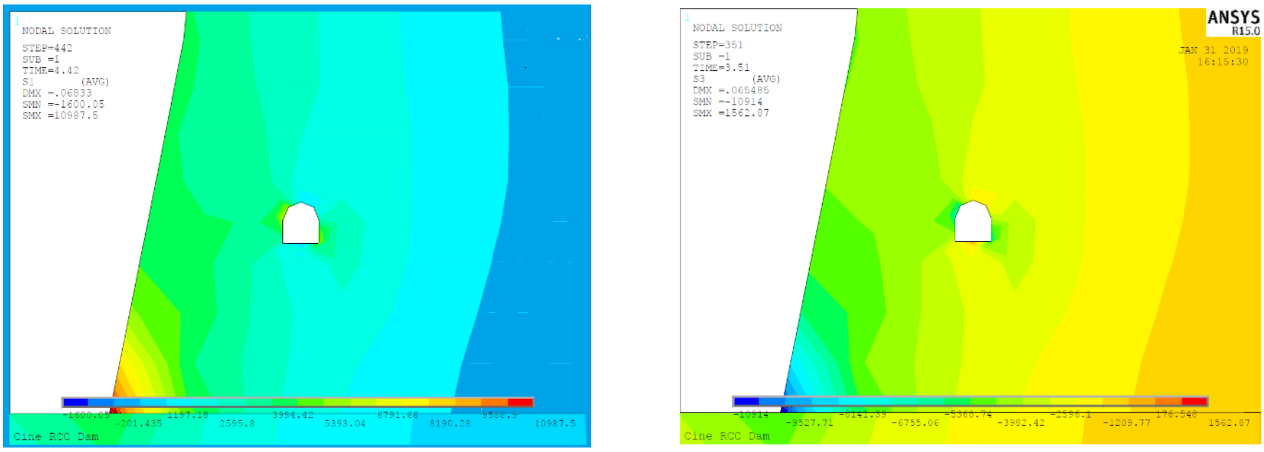

a) t= 4.42 s, max. tensile stress= 6027.8 kPa b) t= 3.51 s, max. compressive stress= - 5949.9 kPa

Fig. 22 Maximum principal stress contour diagrams at bottom gallery in empty reservoir condition

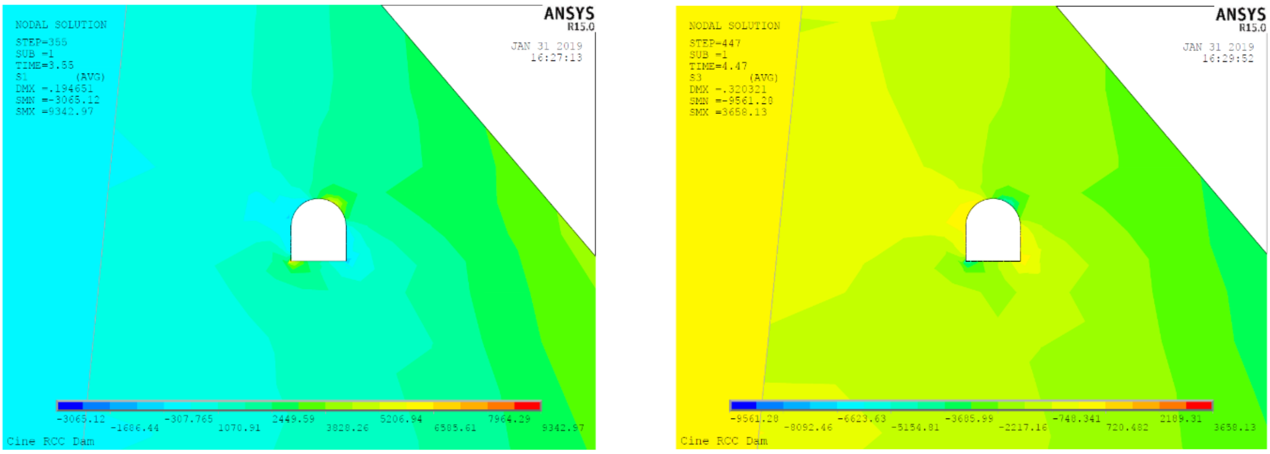

a) t= 3.55 s, max. tensile stress= 6840.7 kPa b) t= 4.47 s, max. compressive stress= - 6139.9 kPa

Fig. 23 Maximum principal stress contour diagrams at upper gallery in full reservoir condition

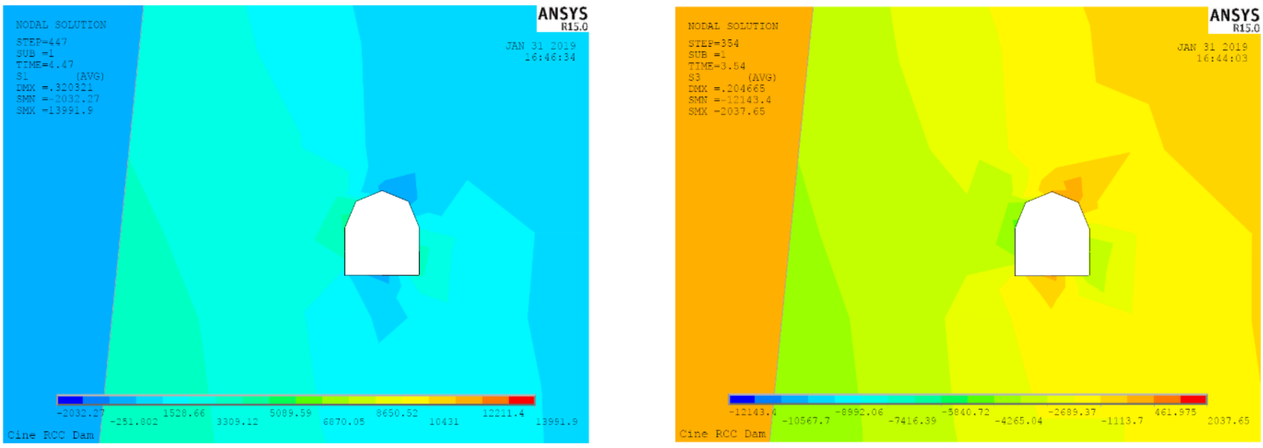

a) t= 4.47 s, max. tensile stress= 4783.4 kPa b) t= 3.54 s, max. compressive stress= -4641.65 kPa

Fig. 24 Maximum principal stress contour diagrams at middle gallery in full reservoir condition

Another important matter in this study is to examine the change of stresses in a certain point if there is a gallery in the dam models. Therefore, Cine dam models with and without gallery in full reservoir case, the stress values in the coordinates of 0.25 m in x axis and the -116.25 m in z axis point that are compared for two cases of dam. As a result of the analysis, the stress value at the selected point in dam model including gallery was 8058.2 kPa and this value was determined as 3794 kPa in dam without gallery in the same location. It is clearly seen that galleries increase the stresses twice therefore the existence of the galleries should not be neglected.

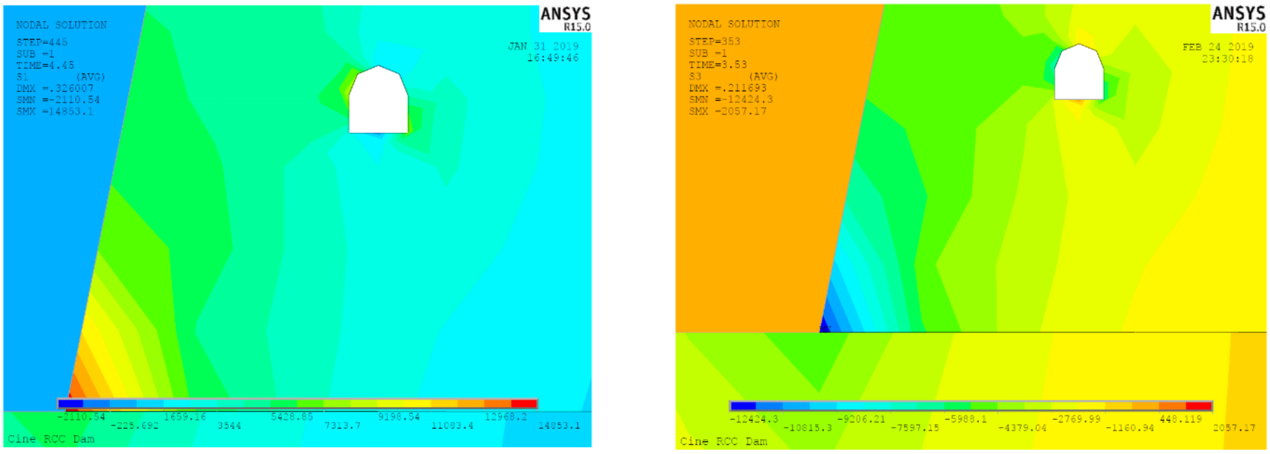

a) t= 4.45 s, max. tensile stress= 8058.2 kPa b) t= 3.53 s, max. compressive stress= -6940.9 kPa

Fig. 25 Maximum principal stress contour diagrams at bottom gallery in full reservoir condition

5. Conclusion

In this study, we investigated the response of the roller compacted concrete dams under ground motion effects. Dam and foundation is considered as linearly elastic. In the numerical analyses, empty and full reservoir conditions are considered. For this purpose, two-dimensional fluid finite elements based on the Lagrangian approach are used.

This study is generally focused on the change of the response because of galleries placed inside the dam. Most of the solutions exclude galleries in the finite element model. We investigated the general reponse of the whole dam and the change of response about galleries. The numerical results clearly appear the existence of galleries change local and global behavior of the dam. Evaluation of the solutions obviously reveal that the existence of galleries must be considered in the numerical analyses of roller compacted concrete dams.

Moreover, according to finite element analyses, the followings can be clearly deducted from this study.

- Hydrodynamic pressure of the reservoir water increases the principle stress components,
- Hydrodynamic pressure of the reservoir water increases the horizontal displacements,
- Hydrodynamic pressure of the reservoir water increases periods of the dam,
- Galleries increases maximum principle stress components in upstream side of the dam,
- Principle stress components increase around the galleries,
- Galleries do not have clear effect on the modal characteristics of the dam at both reservoir cases,
- The principle stresses are quite higher around the galleries compared to ones in the same location of the dam without galleries.
- Galleries must be considered in the finite element model of RCC dams.

References

Abdulrazeg, J., Noorzaei, A.A., Bayagoob, K.H., Jaafar, M.S. and Mohammed, T. A. (2010), "Three dimensional modeling of thermal and structural analysis of roller compacted concrete dam", *9th International Congress on Advances in Civil Engineering*, 27-30 September, Karadeniz Technical University, Trabzon, Turkey.

Akköse, M. (2016), "Arrival direction effects of travelling waves on nonlinear seismic response of arch dams", *Comput. Conc.*, **18**(2), 179-199. https://doi.org/10.12989/cac.2016.18.2.179.

Akpınar, U., Binici, B. and Arıcı, Y. (2014), "Earthquake stresses and effective damping in concrete gravity dams", *Earth. Struct.*, **6**(3), 251-266. https://doi.org/10.12989/eas.2014.6.3.251.

Bayagoob, K.H., Noorzaei, J., Abdulrazeg, A. A., Al-Karni, A. A. and Jaafar M.S. (2009), "Coupled thermal and structural analysis of roller compacted concrete arch dam by three-dimensional finite element method", *Struct. Eng. Mech*, **36**(4), 401-419. https://doi.org/10.12989/sem.2010.36.4.401.

Clough, R. W. and Penzien, J. (1993), *Dynamics of Structures*, 2nd Edn., McGraw-Hill, Singapore.

Erdik, M. (2000), *Report On 1999 Kocaeli and Düzce (Turkey) Earthquakes*, Bogazici University-Department of Earthquake Engineering, http://www.koeri.boun.edu.tr/earthqk/earthqk.html.

Jaafar, M.S., Bayagoob, K.H., Noorzaei, J. and Thanoon, W.A. M. (2007), "Development of finite element computer code for thermal analysis of roller compacted concrete dams", *Adv. Eng. Softw.*, **38**, 886-895. https://doi.org/10.1016/j.advengsoft.2006.08.040.

Karabulut, M. (2016), "Effect of galleries on two dimensional behavior of roller compacted concrete dams", M.Sc. Thesis, Bulent Ecevit University, Zonguldak, Turkey.

Kartal, M.E. (2012), "Three-dimensional earthquake analysis of roller-compacted concrete dams", *Nat. Hazard Earth Sys. Sci.*, **12**(7), 2369-2388. https://doi.org/10.5194/nhess-12-2369-2012.

Kartal, M.E. and Karabulut, M. (2018), "Earthquake performance evaluation of three-dimensional roller compacted concrete dams", *Earth. Struct.*, **14**(2), 167-178. https://doi.org/10.12989/eas.2018.14.2.167.

Kianoush, R., Mirzabozorg, H. and Jalalzadeh, B. (2009), "Damage mechanics approach and modeling nonuniform cracking within finite elements for safety evaluation of concrete dams in 3D space", *Struct. Eng. Mech.*, **33**(1), 31-46. https://doi.org/10.12989/sem.2009.33.1.031.

Lotfi, V. (2007), "Direct frequency domain analysis of concrete arch dams based on FE-BE procedure", *Struct. Eng. Mech*, **26**(4), 363-376. https://doi.org/10.12989/sem.2007.26.4.363.

Moradloo J., Naserasadia, K. and Zamanib, H. (2018), “Seismic fragility evaluation of arch concrete dams through nonlinear incremental analysis using smeared crack model”, *Struct. Eng. Mech.,* **68**(6), 747-760. https://doi.org/10.12989/sem.2018.68.6.747.

Noorzaei, J., Bayagoob, K.H., Thanoon, W.A. and Jaafar, M.S. (2006), “Thermal and stress analysis of Kinta RCC dam”, *Eng. Struct*., **28**, 1795-1802. https://doi.org/10.1016/j.engstruct.2006.03.027.

Sevim, B, Altunışık, A. C. and Bayraktar, A. (2013), “Structural identification of concrete arch dams by ambient vibration tests”, *Adv. Conc. Const.*, **1**(3), 227-237. https://doi.org/10.12989/acc2013.1.3.227.

Sevim, B. (2018), “Geometrical dimensions effects on the seismic response of concrete gravity dams”, *Adv. Conc. Const.*, **6**(3), 269-283. https://doi.org/10.12989/acc.2018.6.3.269.

Su, H., Wen, Z. and Wang, F. (2016), “Fractal behavior identification for monitoring data of dam safety”, *Struct. Eng. Mech.*, **57**(3), 529-541. https://doi.org/10.12989/sem.2016.57.3.529.

USACE (1995), US Army Corps of Engineers. Gravity Dam Design – Engineering and design (engineer manual), EM 1110-2-2200.

Wilson, E.L. and Khalvati, M. (1983), “Finite elements for the dynamic analysis of fluid-solid systems”, *Int. J. Num. Meth. Eng.*, **19**, 1657-1668. https://doi.org/10.1002/nme.1620191105.

Yang, M., Jia, F., Liu, B., Wang, J., Gao, J., Su, H. and Zhao, E. (2017), “A comprehensive evaluation method study for dam safety”, *Struct. Eng. Mech.*, **63**(5), 639-646. https://doi.org/10.12989/sem.2017.63.5.639.

Zienkiewicz, O.C. and Taylor R.L. (1989), *The Finite Element Method*, McGraw-Hill, London, United Kingdom.

Zhang, X., Li, S., Li, Y., Ge, Y. and Li, H. (2011) “Effect of superficial insulation on roller-compacted concrete dams in cold regions”, *Adv. Eng. Softw.*, **42**, 939-943. https://doi.org/10.1016/j.advengsoft.2011.06.004.

Zhuang, D., Ma, K., Tang, C., Cui, X. and Yang, G. (2019), “Study on crack formation and propagation in the galleries of the Dagangshan high arch dam in Southwest China based on microseismic monitoring and numerical simulation”, *Int. J. Rock Mech. Min. Sci*, **115**, 157-172. https://doi.org/10.1016/j.ijrmms.2018.11.016.

CC